Effects of CuO, Cr_2O_3 and Fe_2O_3 Doping on Phase Formation, Microstructure and Electric Properties of $(Ba_{0.85}Ca_{0.15})(Ti_{0.90}Zr_{0.10})O_3$ Ceramics

Surirat Yotthuan[1], Theerachai Bongkarn[1,2*]

[1]Department of Physics, Faculty of Science, Naresuan University, Phitsanulok, 65000, Thailand

[2]Research Center for Academic Excellence in Applied Physics, Faculty of Science, Narasuan University, Phitsanulok, 65000, Thailand

*Corresponding author. E-mail: researchcmu@yahoo.com

ABSTRACT

The effects of CuO, Cr_2O_3 and Fe_2O_3 doping on the phase formation, microstructure and electric properties of $(Ba_{0.85}Ca_{0.15})(Ti_{0.90}Zr_{0.10})O_3$ (BCTZ) ceramics prepared by the combustion method were studied. Glycine was used as fuel and the ratio of raw material to fuel was 1:1.11. All samples were calcined and sintered at the temperatures of 1050°C and 1450°C for 2 h, respectively. The XRD data showed a pure perovskite structure with the coexistence of orthorhombic and tetragonal phases in all samples. The grain morphology of the ceramics exhibited irregular polyhedron shape and the average grain size was in the range of 15.5±0.9 to 42.8±2.2 µm. Samples of the BCTZ ceramics modified with Cu exhibited the highest density (5.79 g/cm^3), the highest maximum dielectric constant (ε_c=12500) and good ferroelectric properties (P_r=12.6 µC/cm^2 and E_c=2.5 kV/cm).

Keywords: phase formation, microstructure, dielectric properties, ferroelectric properties

INTRODUCTION

$(Ba_{0.85}Ca_{0.15})(Ti_{0.90}Zr_{0.10})O_3$ (BCTZ) solid solution is one of the lead-free piezoelectric materials with a perovskite structure, which has received considerable attention. This is mainly due to their high piezoelectric coefficient ($d_{33}\geq$442 pC/N) around a morphotropic phase boundary (MPB). Moreover, BCTZ ceramics show good dielectric properties (ε_r>2800 and ε_m>10000) and remnant polarization (P_r~9.43 µC/cm^2) with the use of high calcination (1300-1350 ºC) and sintering temperatures (1500-1550 ºC) as well as very long dwell times (Wu *et al*, 2012; Liu *et al*, 2009) In recent years, methods that can reduce the firing temperature and improve the electrical properties have been studied by using doping material, including metal oxides such as CuO (Sun *et al*, 2015), Fe_2O_3 (ZuO *et al*, 2008), ZnO (Zhao *et al*, 2015), MgO (Miao *et al*, 2015) and Cr_2O_3 (Wei *et al*, 2015). It is well known that doping with these metal oxides helps to produce the liquid phase during the sintering process, which promotes densification and better grain morphology. T. Bongkarn and coworkers (Bongkarn *et al*, 2016) prepared $(K_{0.44}Na_{0.52}Li_{0.04})(Nb_{0.84}Ta_{0.10}Sb_{0.06})O_3$ (KNLNTS)

ceramic with added Fe_2O_3 (0-1.0 wt%) by the solid state reaction method. The results concluded that Fe_2O_3 doped at 0.6 wt% increased the electrical properties (ε_r~2800 and ε_C~7500) and ferroelectric properties (P_r~27.9 μC/cm^2 and E_c~9.9 kV/cm), which were higher than undoped KNLNTS ceramic. J. Wei and coworkers (Wei *et al.*, 2015) found that doping Cr_2O_3 into $Bi_{0.8}Ba_{0.2}FeO_3$ (BBFC) ceramic obtained good ferroelectric properties of P_r~0.95 μC/cm^2 which were higher than undoped BBFC ceramic. F. Azough and coworkers (Azough *et al.*, 2011) investigated CuO doped $Na_{0.475}K_{0.475}Li_{0.05}NbO_3$ (NKLN) ceramics produced by the mixed oxide route. The results showed that the CuO doping decreased the sintering temperature of NKLN and increased the density to within 96% of the theoretical value. With CuO doping of 0.4 wt%, the ceramic exhibited a saturation polarization (P_s) of 30 μC/cm^2, remanent polarization (P_r) of 27 μC/cm^2 and coercive field (E_c) of 1.0 kV/mm.

In this research, we studied the phase formation, morphology and electrical properties of BCTZ ceramics modified by doping with 0.4 wt% of CuO, Cr_2O_3 and Fe_2O_3, synthesized by the solid state combustion technique.

EXPERIMENTAL

$(Ba_{0.85}Ca_{0.15})(Ti_{0.90}Zr_{0.10})O_3$ (BCTZ) doped with 0.4 wt% of Fe_2O_3 (BCTZ-Fe), CuO (BCTZ-Cu) and Cr_2O_3 (BCTZ-Cr) ceramics were prepared by the solid-state combustion method with glycine used as the fuel. High purity $Ca(NO_3)_2.4H_2O$, $BaCO_3$, TiO_2, and ZrO_2 were used as raw materials. The raw materials were weighed according to the desired stoichiometry and mixed by ball milling using ethanol as medium for 24 h. After that, the slurry was dried at 90 ºC and mixed with glycine at a ratio of 1:1.11 in an agate mortar. Next, the mixed powders were calcined at a temperature of 1050 ºC for 2 h (Kornphom *et al*, 2016). The calcined BCTZ powders were mixed with Fe_2O_3, CuO and Cr_2O_3 powders at ratios of 0.4 wt% in all samples. These compound powders were ball milled with a polyvinyl alcohol (PVA) for 12 h. Next, the powders were dried and pressed into pellets with a diameter of ~15 mm and a thickness of ~1.2-1.4 mm at 80 MPa. Pellets were sintered at 1450 ºC for 2 h in a sealed alumina crucible (Kornphom *et al.*, 2016). Subsequently, for electrical measurements, the sintered samples were polished and painted with silver paste on both sides and fired at 500 ºC for 15 min.

The phase structures of the sintered ceramics were analyzed using X-ray diffraction (XRD). The microstructures of the ceramics were studied using a scanning electron microscope (SEM). The density of the all sintered ceramics was measured by the Archimedes method. The dielectric constant and dielectric loss of the ceramics were measured by an LCR meter at a frequency of 1 kHz over a temperature range from 25 ºC to 200 ºC. The ferroelectric polarization hysteresis loops (P-E) were measured using a computer controlled modified Sawyer-Tower circuit.

RESULTS AND DISCUSSION

Fig. 1 (a) illustrates the XRD spectra of the BCTZ, BCTZ-Cu, BCTZ-Fe and BCTZ-Cr ceramics sintered at 1450 º for 2 h, measured at room temperature in the 2θ range of 10-70º. A pure perovskite phase was formed for all samples, and no impurity phase can be found in the XRD peak. Fig. 1 (b) and (c) shows the expanded XRD spectra of all samples at the 2θ angle of 38-40º and 43-47º. Generally, the characteristics of the orthorhombic phase (O) in the X-ray diffraction spectral (in accordance with JCPDS no. 81-2200) demonstrates dual peaks of $(102)/(120)_O$ and $(022)/(200)_O$ at a 2θ range of 39º and 45º while the tetragonal phase (T) (in accordance with JCPDS no. 74-1960) exhibits a single peak of $(111)_T$ at 2θ around 39º and dual peaks of $(002)/(200)_T$ around 45º. In this study, the XRD peak of the BCTZ ceramics presented no symmetry peak at 2θ around 39º (Fig. 1 (b) I) and dual peaks were not observed at 2θ around 45º (Fig. 1 (c) I). These results suggest that the orthorhombic and tetragonal phases coexist in this composition. For BCTZ-Cu, BCTZ-Cr and BCTZ-Fe ceramics, the diffraction peaks of these ceramics showed a more non-symmetry peak (skewed to left side) and a slight move to a lower angle (Fig. 1 (b) II-IV). Broader dual peaks were also observed at 2θ around 45º (Fig. 1 (c) II-IV). These results suggest that these compositions still had coexisting phases (O+T) and the unit cell expanded.

SEM micrographs of the samples are shown in Fig. 2 (a)-(d). The grains of all ceramics exhibited irregular polyhedron shapes, and the grain growth tended to be anisotropic. The BCTZ ceramics showed large grains with a uniform distribution and were closely packed (Fig. 2 (a)). Similar to BCTZ, BCTZ-Cu ceramic also showed a uniform grain distribution with larger grain sizes (Fig. 2 (b)). In the case of the BCTZ-Cr ceramic, it exhibited larger grain sizes compared to BCTZ ceramics, a non-uniform grain distribution and pores on the surface (Fig. 2 (c)). The increased grain size of BCTZ-Cu and BCTZ-Cr ceramics may be caused by the presence of oxygen vacancy that helps mass transport during the sintering process, which is similar to previous results (Chen *et al.*, 2015). Compared with BCTZ ceramics, the BCTZ-Fe ceramic shows smaller grain size and small pores at the grain boundaries. This result suggested that Fe_2O_3 may accumulate at the grain boundaries and suppressed the grain growth of the BCTZ ceramic (Fig. 2 (d)) (Ma *et al.*, 2013). The average grain sizes were 37.8±5.5, 42.8±2.2, 36.9±3.9 and 15.5±0.9 μm for BCTZ, BCTZ-Cu, BCTZ-Cr and BCTZ-Fe ceramics, respectively. The measured density of all samples was obtained by the Archimedes method. The values of the density and relative density of the samples are listed in Table 1. The highest density and relative density of 5.79 g/cm^3 and 98.3% were obtained by the BCTZ-Cu ceramic. The measured density results corresponded well with the SEM results.

The temperature dependence of the dielectric behavior at 1 kHz of BCTZ, BCTZ-Cu, BCTZ-Cr and BCTZ-Fe ceramics sintered at 1450 ºC for 2 h is displayed in Fig. 3. The BCTZ ceramic showed two dielectric anomalies. The first peak appeared at a lower temperature of 36 ºC, which corresponded to a phase transition from the orthorhombic ferroelectric phase to the tetragonal ferroelectric phase (T_{O-T}). The second peak was observed at a higher temperature ~ 109 ºC which was related to the phase transition from tetragonal ferroelectric phase to cubic paraelectric phase (T_c). Similar to BCTZ, the BCTZ-Cu and BCTZ-Cr ceramics showed two phase transitions as a function of temperature. The T_{O-T} and T_C values of BCTZ-Cu and BCTZ-Cr ceramics are shown in Table 1. In contrast to BCTZ, BCTZ-Cu, and BCTZ-Cr, the BCTZ-Fe ceramics exhibited only one dielectric peak at T_c (~ 78 ºC). The absence of a T_{O-T} transition may be attributed to the lattice distortion in the crystal structure. The T_{O-T} of all samples with different dopants are presented in the inset of Fig. 3 (a)-(d). The ε_r of all samples were in the range of 1790-3097, as shown in Table 1. The BCTZ-Cu ceramic showed the highest dielectric constant (ε_c=12500) and the low dielectric loss (tan δ at T_c = 0.017). The values of the dielectric loss at room temperature (T_r) and T_c are shown in Table 1. The dielectric properties corresponded to the morphology and density results.

In addition, BCTZ ceramics exhibited a sharp dielectric curve at T_c (Fig. 3 (a)). While for the BCTZ-Cu, BCTZ-Cr and BCTZ-Fe ceramics, the dielectric curve at T_c become broader when compared with undoped ceramics (Fig. 3 (b)-(d)). This indicated that a diffuse phase transition was formed. A modified Curie-Weiss law (Uchino *et al*., 1982; Ding *et al*., 2009) can be used to described the diffuseness of the phase transition at T_c, as described by

$$\frac{1}{\varepsilon_r} - \frac{1}{\varepsilon_c} = (T - T_c)^{\gamma} (T > T_c) / C$$

Where ε_c is the maximum value of the dielectric constant at T_c, C is the Curie-Weiss constant and γ is the diffusion factor ($1 < \gamma < 2$, 1 and 2 are corresponding to normal ferroelectric and relaxor ferroelectric, respectively) (Ciomaga *et al.*, 2007). Plots of $\ln\left(1/\varepsilon - 1/\varepsilon_c\right)$ as a function of $\ln\left(T - T_c\right)$ are shown in Fig. 4 (a)-(d) and the values of γ for all samples were obtained. In all calculations, the γ values of BCTZ-Cu, BCTZ-Cr, and BCTZ-Fe ceramics were higher than the BCTZ ceramic (Fig. 4 (a)-(d)). This indicated that these samples exhibited an increasing in relaxor ferroelectric behavior. The increasing of the relaxor ferroelectric state in BCTZ-Cu, BCTZ-Cr, and BCTZ-Fe ceramics could be caused by a distortion of the crystal lattice owing to the generation of oxygen vacancies (Miao *et al.*, 2015).

Polarization hysteresis loops of the BCTZ, BCTZ-Cu, BCTZ-Cr and BCTZ-Fe ceramics were measured at room temperature, as shown in Fig. 5. The P-E loop of the BCTZ ceramic showed a slim and saturated curve. The remanent polarization (P_r) and coercive field (E_c) of the BCTZ ceramic are 10.14 μC/cm^2 and 2.90 kV/cm. Similar to BCTZ, the BCTZ-Cu and BCTZ-Fe ceramics showed slim and saturated loops. The ferroelectric properties of the BCTZ-Cu ceramic were better than the BCTZ ceramic (P_r=12.64 μC/cm^2 and E_c=2.47 kV/cm). In contrast, the BCTZ-Fe ceramic ferroelectric properties were degraded (Table 1). Unlike the BCTZ, BCTZ-Cu and BCTZ-Fe ceramics, the loop of the BCTZ-Cr ceramic becomes unsaturated which indicated a leakage current was produced (P_r=16.41 μC/cm^2 and E_c=6.57 kV/cm). In this work, samples of the BCTZ modified with Cu-induced good dielectric and ferroelectric behavior. This behavior can be attributed to the well-developed microstructure and the highest density of this sample. The microstructure enhanced the domain variants while the trapping of space charges at the boundaries was reduced, which makes domain reorientation easier (Bongkarn *et al*., 2016; Jha *et al*., 2009).

CONCLUSION

In this work, we investigated the effects of CuO, Cr_2O_3 and Fe_2O_3 doping on the phase formation, microstructure and electrical properties of BCTZ ceramics fabricated by the solid state reaction combustion technique. A pure perovskite phase and a morphotropic phase boundary between the orthorhombic and tetragonal phase were found in all samples. Compared with BCTZ ceramics, BCTZ-Cu and BCTZ-Cr ceramics exhibited a larger grain size while BCTZ-Fe showed a smaller grain size. Doping of Cu can improve the density and microstructure of BCTZ ceramics, caused by the presence of oxygen vacancies that helps mass transport during the sintering process. The BCTZ-Cu ceramic demonstrated a good morphology, the highest density (5.79 g/cm^3), the highest maximum dielectric constant (ε_c=12500) and good ferroelectric properties (P_r=12.6 μC/cm^2 and E_c=2.5 kV/cm). All the results of the morphology, density, electrical and ferroelectric are consistent with each other.

ACKNOWLEDGEMENTS

The authors wish to thank the Department of Physics, Faculty of Science, Naresuan University for their supporting facilities. This work was supported by the Higher Education Research Promotion and National Research University Project of Thailand, Office of the Higher Education Commission. Thanks are also given to Dr. Kyle V. Lopin for his help in editing the manuscript.

REFERENCES

Wu, J., Xiao, D., Wu, W., Chen, Q., Zhu, J., Yang, Z., and Wang, J. (2012) . Composition and poling condition-induced electrical behavior of $(Ba_{0.85}Ca_{0.15})(Ti_{1-x}Zr_x)O_3$ lead-free piezoelectric ceramics. *J. Eur. Ceram. Soc., 32,* 891-898.

Liu, W., and Ren, X. (2009). Large piezoelectric effect in Pb-Free ceramics. *Phys. rev. lett., 103,* 257602.

Sun, H., Zhang, Y., Liu, X., Liu, Y., and Chen, W. (2015). Effects of CuO additive on structure and electrical properties of low-temperature sintered $Ba_{0.98}Ca_{0.02}Zr_{0.02}Ti_{0.98}O_3$ lead-free ceramics. *Ceram. Int., 41,* 555-565.

Zuo, R., Xu, Z., and Li, L. (2008). Dielectric and piezoelectric properties of Fe_2O_3-doped $(Na_{0.5}K_{0.5})_{0.96}Li_{0.04}Nb_{0.86}Ta_{0.1}Sb_{0.04}O_3$ lead-free ceramics. *J. Phys. Chem. Solids., 69,* 1728-1732.

Zhao, Z., Li, X., Ji, H., Dai, Y., and Li, T. (2015). Microstructure and electrical properties in Zn-doped $Ba_{0.85}Ca_{0.15}Ti_{0.90}Zr_{0.10}O_3$ piezoelectric ceramics. *J. Alloy. Compd, 637,* 291-296.

Miao, J., Zhang, Z., Liu, Z., and Li, Y. (2015). Investigation on the dielectric properties of Mg-doped $(Ba_{0.95}Ca_{0.05})(Ti_{0.85}Zr_{0.15})O_3$ ceramics. *Ceram. Int., 41,* S487-S491.

Wei, J., Zhang, M., Deng, H., Chu, S., Du, M., and Yan, H. (2015). Effect of Cr doping on ferroelectric and magnetic properties of $Bi_{0.8}Ba_{0.2}FeO_3$. *Ceram. Int., 41,* 8665-8669.

Bongkarn, T., Chootin, S., Pinitsoontorn, S., and Maensiri, S. (2016). Excellent piezoelectric and ferroelectric properties of KNLNTS ceramics with Fe_2O_3 doping synthesized by the solid state combustion technique. *J. Alloy. Compd., 682,* 14-21.

Azough, F., Wegrzyn, M., Freer, R., Sharma, S., and Hall, D. (2011). Microstructure and piezoelectric properties of CuO added (K, Na, Li)NbO_3 lead-free piezoelectric ceramics. *J. Eur. Ceram. Soc., 31,* 569-576.

Kornphom, C., Vittayakorn, N., and Bongkarn, T. (2016). Low firing temperatures and high ferroelectric properties of $(Ba_{0.85}Ca_{0.15})(Ti_{0.90}Zr_{0.10})O_3$ lead-free ceramics synthesized by the combustion technique. *Ferroelectrics., 491(1),* 44-53.

Chen, X., Ruan, X., Zhao, K., He, X., Zeng, J., Li, Y., Zheng, L., Park, C. H., and Li, G. (2015). Low sintering temperature and high piezoelectric properties of Li-doped (Ba, Ca)(Ti, Zr)O_3 lead-free ceramics. *J. Alloy. Compd., 632,* 103-109.

Ma, J., Liu, X., and Li, W. (2013). High piezoelectric coefficient and temperature stability of Ga_2O_3-doped $(Ba_{0.99}Ca_{0.01})(Zr_{0.02}Ti_{0.98})O_3$ lead-free ceramics by low-temperature sintering. *J. Alloy. Compd., 581,* 642-645.

Uchino, K., and Nomura, S. (1982). Critical exponents of the dielectric constants in diffused-phase-transition crystals. *Ferroelectrics., 44,* 55-61.

Ding, S. H., Chen, T., and Song, T. X., (2009). Dielectric properties of $Ba(Ti_{0.91}Zr_{0.009})O_3$ ceramics doped with CuO. *Ferroelectrics., 383,* 159-165.

Ciomaga, C., Viviani, M., Buscaglia, M. T., Buscaglia, V., Mitoseriu, L., Stancu, A., and Nanni, P. (2007). Preparation and characterization of the Ba(Zr, Ti)O_3 ceramics with relaxor properties. *J. Eur. Ceram. Soc., 27,* 4061.

Jha, P. A., and Jha, A. K. (2012). Influence of processing conditions on the grain growth and electrical properties of barium zirconate titanate ferroelectric ceramics. *J. Alloy. Compd., 513,* 580-585.

Table Captions

Table 1 Data of density, transition temperatures and electrical properties of BCTZ, BCTZ-Cu, BCTZ-Cr and BCTZ-Fe ceramics.

Figure Captions

Fig. 1 XRD spectra of BCTZ, BCTZ-Cu, BCTZ-Fe and BCTZ-Cr ceramics in the 2θ range of; (a) 10-70º, (b) 38-40º and (c) 43-47º.

Fig. 2 SEM micrographs of polished and thermal etched surface of sintered (a) BCTZ, (b) BCTZ-Cu, (c) BCTZ-Cr and (d) BCTZ-Fe

Fig. 3 Temperature dependence of dielectric constant and dielectric loss for the samples measured at 1 kHz; (a) BCTZ, (b) BCTZ-Cu, (c) BCTZ-Cr and (d) BCTZ-Fe

Fig. 4 The plots of $\ln(1/\varepsilon - 1/\varepsilon_c)$ against $\ln(T - T_c)$ at 1 kHz for the BCTZ, BCTZ-Cu, BCTZ-Cr and BCTZ-Fe ceramics

Fig. 5 Polarization hysteresis loops of the BCTZ, BCTZ-Cu, BCTZ-Cr and BCTZ-Fe ceramics at room temperature under the electric field of 40 kV/cm.

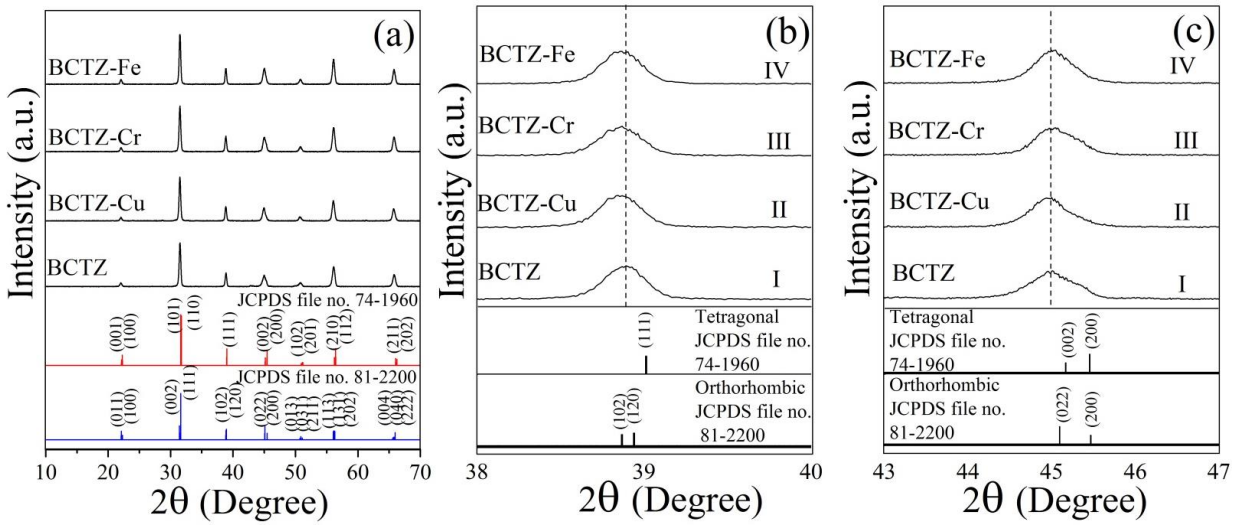

Fig. 1 XRD spectra of BCTZ, BCTZ-Cu, BCTZ-Fe and BCTZ-Cr ceramics in the 2θ range of; (a) 10-70º, (b) 38-40º and (c) 43-47º

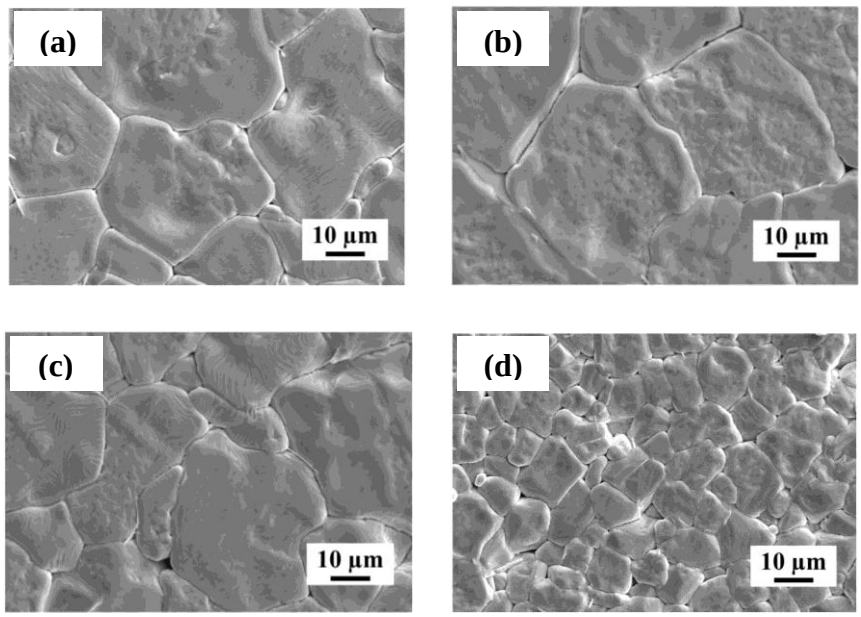

Fig. 2 SEM micrographs of polished and thermal etched surface of sintered (a) BCTZ, (b) BCTZ-Cu, (c) BCTZ-Cr and (d) BCTZ-Fe

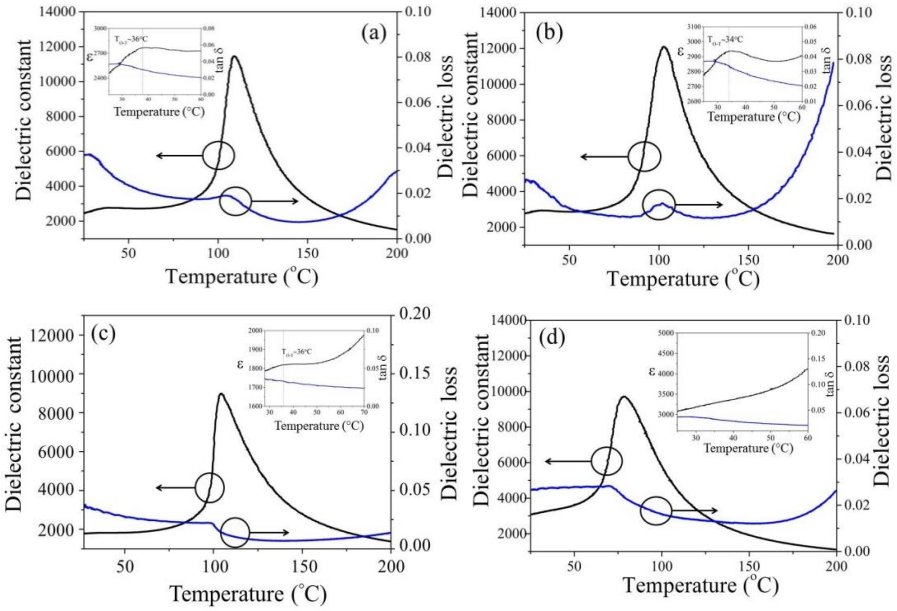

Fig. 3 Temperature dependence of dielectric constant and dielectric loss for the samples measured at 1 kHz; (a) BCTZ, (b) BCTZ-Cu, (c) BCTZ-Cr and (d) BCTZ-Fe

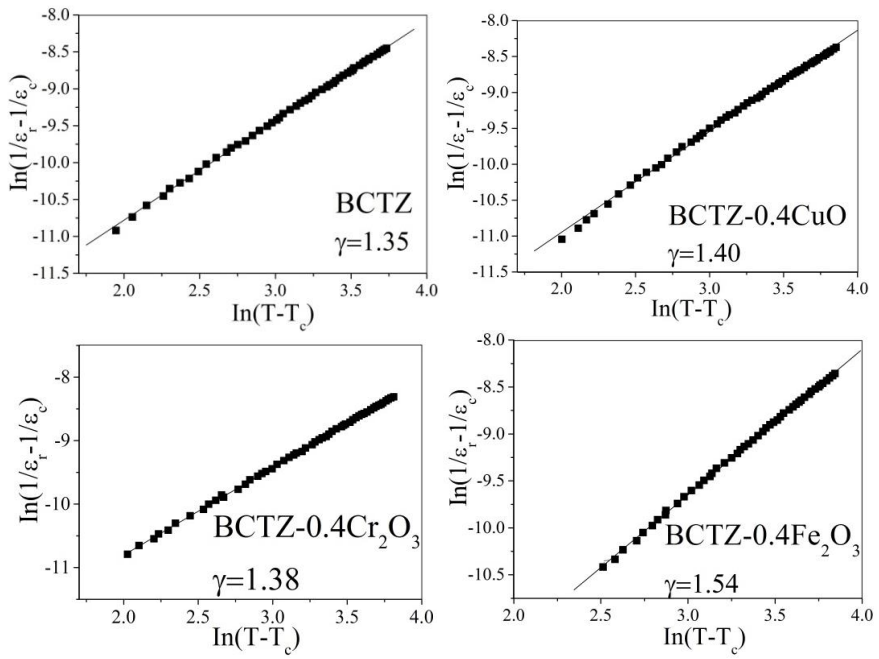

Fig. 4 The plots of $\ln(1/\varepsilon - 1/\varepsilon_c)$ against $\ln(T - T_c)$ at 1 kHz for the BCTZ, BCTZ-Cu, BCTZ-Cr and BCTZ-Fe ceramics

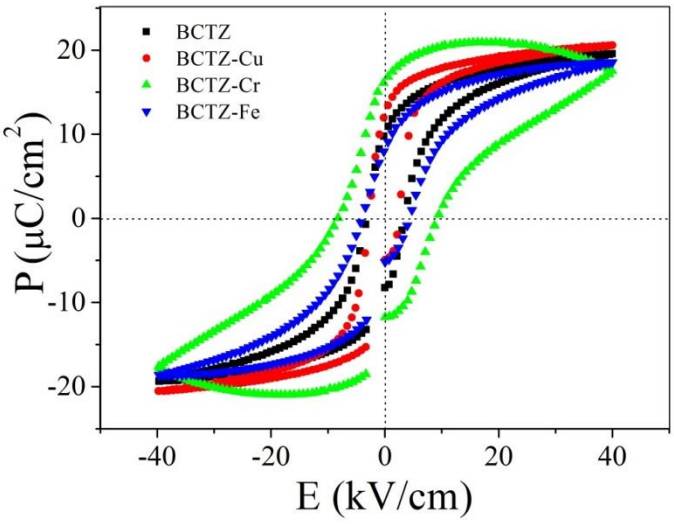

Fig. 5 Polarization hysteresis loops of the BCTZ, BCTZ-Cu, BCTZ-Cr and BCTZ-Fe ceramics at room temperature under the electric field of 40 kV/cm

Sample	Density (g/cm^3)	Relative density (%)	T_{O-T} (°C)	T_c (°C)	ε_r	tan δ at T_r	ε_c	tan δ at T_c	P_r ($\mu C/cm^2$)	E_c (kV/cm)
BCTZ	5.71	96.95	36	109	2964	0.087	11863	0.019	10.14	2.90
BCTZ-Cu	5.79	98.30	34	104	2951	0.017	12514	0.017	12.64	2.47
BCTZ-Cr	5.61	95.25	36	104	1790	0.037	8984	0.014	16.41	6.57
BCTZ-Fe	5.69	96.60	-	78	3097	0.026	10097	0.042	8.42	4.41

Table 1 Data of density, transition temperatures and electrical properties of BCTZ, BCTZ-Cu, BCTZ-Cr and BCTZ-Fe ceramics.